Infrared wireless network sensors for imminent forest fire detection

Ignacio Bosch Roig
Institute of Telecommunications and Multimedia Applications (iTEAM)
Universidad Politécnica de Valencia
Valencia, Spain
igbosroi@dcom.upv.es

Luis Vergara Domínguez
Institute of Telecommunications and Multimedia Applications (iTEAM)
Universidad Politécnica de Valencia
Valencia, Spain
lvergara@dcom.upv.es

Abstract **- This paper presents an automatic forest fire surveillance ground system applied to early fire detection. Sensor wireless network scheme allows not only supervising remotely wide-forest area, but also to detect immediately any fire threat. A real system for forest fire detection in actual operation is presented. The system is based on advanced thermal image processing techniques with the purpose of determining the presence of fire. The projected system performs the fusion of different detectors, which exploit different expected characteristics of a real fire, like persistence and increase in time. Theoretical results, practical simulations and results in a real environment are presented to corroborate the control of the probability of false alarm (PFA) and to evaluate the probability of detection (PD) dependence on signal to noise ratio (SNR). Delays of the system for alarm detection of controlled fire have been also evaluated. And finally, temporary evolution of false and true alarms is presented to evaluate the long-term performance in a real environment.**

Keywords - Infrared sensors, image processing, fire detection

I. INTRODUCTION

Video surveillance by means of sensor technologies is of great interest when monitoring wide forest areas. Video sensors and particularly thermal sensors [1] constitute a powerful tool to automate and complement human capabilities in wide-area surveillance tasks, since human capabilities are limited, among others, by the decrease of vision perception and by the range of coverage area. There is no need to comment on the importance of this type of systems for the protection and conservation of natural spaces [2]

Studies on forest fire detection and different contributions have been developed in the past. They have in general, several practice limitations. We can cite, among others, satellite based applications [3], but they are time limited when continuous surveillance over the same area is required [4]. Visible light cameras applications [5] but they are limited by the decreasing of vision perception at night [6]. And infrared based systems [7], [8] and [9] but in this kind of systems, signal processing algorithms are calibrated in a rather empirical manner, without relating to optimum filtering or detection theory.

So an automatic forest fire surveillance wireless system based on infrared sensors is presented at this paper in which we have introduced some significant innovations regarding classical infrared based systems. Basically, the algorithms are selected inside the framework of optimum statistical signal processing theory. Optimality is in the sense of the Neyman-Pearson criterion: given a selected Probability of False Alarm (*PFA*), try to maximize the Probability of Detection (*PD*). In our scheme, we have total control of the *PFA* because we have knowledge of the statistical distribution of every statistic involved in it. Also the *PD* is maximized by appropriate selection of different energy detectors, which are known to be optimum under very general models of the background noise and of the unknown signal to be detected. Therefore, the proposed system provides total control of a tolerable level of false alarms and has maximum sensitivity to the presence of an uncontrolled fire for the defined false-alarm rate. In the end, this implies a greater detection range and greater reliability of the overall system.

In this paper, we focus on how to process the images captured from each infrared sensor with simulated and real experiences. In Section 2, a description of the global system is presented. In Section 3 a scheme for infrared image processing is presented. In Section 4 the theoretical basis is corroborated with practical simulations. In Section 5 a prototype system and some real data results are presented, and finally, some conclusion about the operation of the system will be also offered.

II. GLOBAL SYSTEM

The implemented system has two types of stations; several local stations strategically located to render a required coverage and a central station, see Figure 1. The local stations have three basic stages: a first stage of thermal and visible image capture, a second stage of image processing, and a third stage of communications.

Since the system has been designed to work in wide forest areas and the required number of sensors and its location depend on the concrete scenario, it is important to choose a scalable technology system. For all these reasons, we have used an infrared sensor network based on a wireless

communication link in order to collect all the sensor information in a central station.

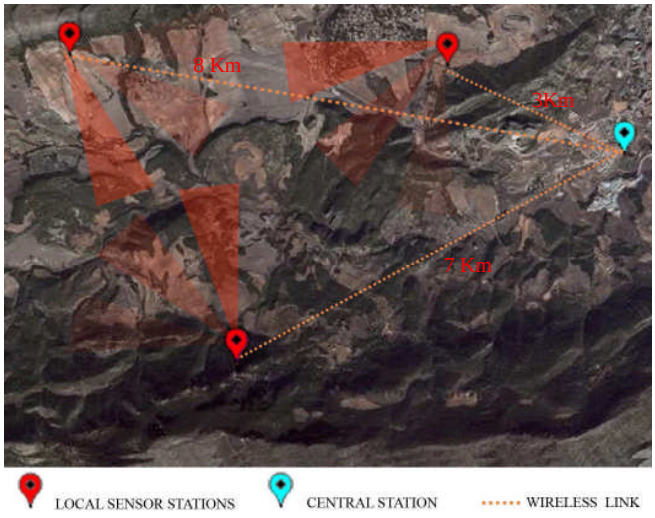

Figure 1. Global System diagram.

The local sensor station main functions are data acquisition (from each of the sensor belonging to the monitoring network) and real time image processing.

An acquisition card captures the images from the IR sensor. The captured images will be the input data to the image-processing step. Furthermore, another camera in the video range is used to provide visible access to the area under surveillance. If an alarm is detected, the system captures both thermal image and a visible one, which only contributes to information if there is sufficient diurnal light. In spite of the automatic operation of the system, both cameras can be remotely controlled in manual mode in order to change system parameters or to verify the detected fire threats. See Figure 2.

The thermal cameras which are used can be low cost and without the ability to show temperature values, they do not require the specific values of temperature, but rather the relative increments of infrared energy in every pixel with respect to some properly defined reference level.

Moreover, the proposed system indirectly uses physical properties of the environment (such as temperature) to reduce false alarms. In the calibration stage, the system adjusts the sensitivity based on numerical parameters such as level and span, which are supplied by the infrared camera. These have a direct correspondence with physical temperature values.

The thermal images captured from each sensor are processed in real time to meet temporal restrictions and to minimize the information flow as discussed below in section 3. Therefore, the communication unit performs the management for a correct transmission of this basic information.

For example, if a possible fire is detected, an alarm must be sent to the central station indicating the geographic location of the fire in minimum time and optimizing the communication resources. To avoid an excessive flow of information, only alarm threat coordinates, together with complementary time-space information, are sent from the local station to the central station.

Figure 2. Real global system with infrared/visible cameras and wireless comunication unit

In addition, an optimized system of alarm information compression has been implemented to transmit only the contour of the form of the object described by the alarms, when they are numerous and close to each other.

The wireless link manages the information transmission between each sensor of the network and the central station. The central station represents fire threats in a zone map by means of a Geographic Information System (GIS), or any other equivalent form for locating alarms in a given area. The central station also performs other functions, such us management of historic alarm data-bases or remote connection to surveillance ports. In addition, all the control parameters of the system can be modified in real time by the central station through of communications unit. Finally, note that the system has control of the thresholds of each detector type, which are calculated from the desired *PFA* and from the sensitivity of the system, which depends on the level and the span obtained from the camera in each recalibration. This allows the thresholds to change based on the different seasons and the different weather conditions, such as morning, afternoon, night, summer, winter, etc.

III. PROCESSING THE IMAGES FROM INFRARED SENSORS

We focus on processing the thermal images from each local sensor, as described above. We perform a pixel to pixel processing. We turn each thermal image into a matrix of pixels, where each pixel is associated with a resolution cell corresponding to certain coordinates of rank and azimuth. In this way, we generate a vector that describes the time history of each resolution cell (see Figure 3).

A first approximation to the problem of automatic alarms detection could be to decide the presence of fire, in one resolution cell, when the energy level of the pixel under test reaches a certain threshold. If the statistic distribution of the

noise is known, the threshold can be fitted to satisfy a desired probability of false alarm (PFA), getting a probability of detection (PD) that depends on the signal to noise ratio (SNR).

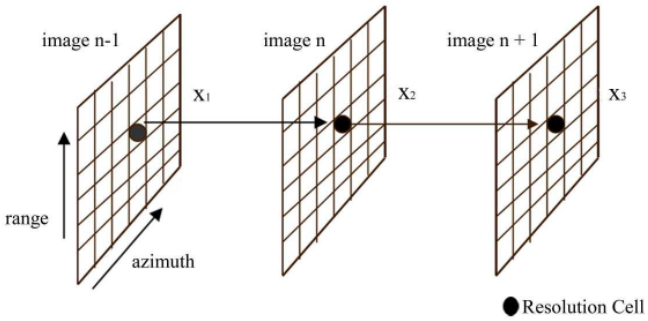

Figure 3. Temporal processing of resolution

On the other hand, usually, infrared noise registered from wide-area surveillance (registered values from usual environment conditions, without considering fires), is highly correlated, that is: the temperature among neighbor cells, and for the same cell along successive images, changes slowly. We can take advantage of this additional information about infrared background noise to improve the SNR using a noise predictor. The noise predictor will compute the noise level of the cell under test, through different scans. Then, this estimated level may be subtracted from the pixel under test, thus improving SNR. Note that if we improve the SNR we get a better PD for a given PFA.

The proposed ideas are applied in the detector scheme of Figure 4. The detector is applied to each resolution cell.

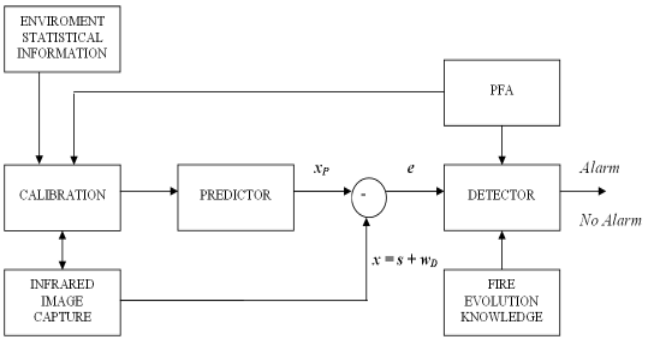

Figure 4. Uncontrolled fires detector general scheme

Partial aspects of the algorithms were previously presented. In [10] the design of an optimum linear predictor was considered. The input to the linear predictor was the values of the pixel under analysis recorded in previous scans. In [11] the linear predictor is extended to the non-gaussian case by including a nonlinear gain. Also in [10] a matched subspace detector is considered to suppress undesired alarms due to "occasional" effects like cars, people or wind. In [12] the matched subspace detector is complemented with an increase detector to take advantage of the expected increasing temperature behavior of an uncontrolled fire. Fusion of the decisions made by both detectors is also considered in [12]. Finally in [13] a complete detector scheme is proposed, which makes use of both detectors, but considering a different time-scale for everyone. Thus several matched subspace detectors corresponding to short-term intervals are fused to give the so-called persistence decision. Then a long-term increasing detector is implemented, to give the increase decision. Finally both decisions are fused.

In the system described in this paper we have basically implemented the detector scheme of [12] plus a linear predictor, which uses a reference image for prediction instead of the previous images as it was done in [10].

In the following we include a brief explanation of the algorithms. More specific details may be found in the mentioned references. A main objective is to have control of the overall PFA achieved; hence we present some new simulation to verify the capability of controlling the overall PFA in the complete detector system. And also we presented a dependence study of PFA and PD with the system parameters.

The input signal to the scheme is the vector $\mathbf{x} = \mathbf{s} + \mathbf{w_D}$ containing the level of one resolution cell through D consecutive image scans. So, $\mathbf{x}$ will always have a noise component $\mathbf{w_D}$ and when a true alarm is presented, the vector $\mathbf{x}$ will also contain the signal component $\mathbf{s}$ due to the presence of a fire. In order to improve the signal to noise ratio (SNR) of $\mathbf{x}$, a reference image is also computed. This image represents the infrared scene noise computed from N consecutive scans of the cell under test, assuming that there is no signal present at those scans. Then, we predict $\mathbf{w_D}$ from the reference image, using a predictor (details about the optimum design of the predictor could be seen at [10]). Subtracting the prediction $\mathbf{x_p}$ from the signal $\mathbf{x}$ we get vector $\mathbf{e}$ that defines the detector input with improved SNR.

An uncontrolled fire is supposed to be a fire that persists on time, increasing continuously their temperature, in contrast with other occasional effects like cars or atmospheric changes that may produce undesired alarms (see Figure 5).

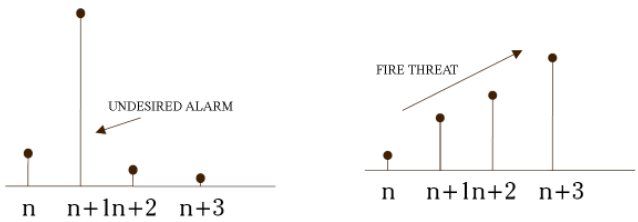

Figure 5. Uncontrolled fire vs undesired false alarm pattern

This consideration let us to propose the detector scheme of Figure 6. This scheme exploits the assumption about persistence and increase by means of decision fusion algorithms.

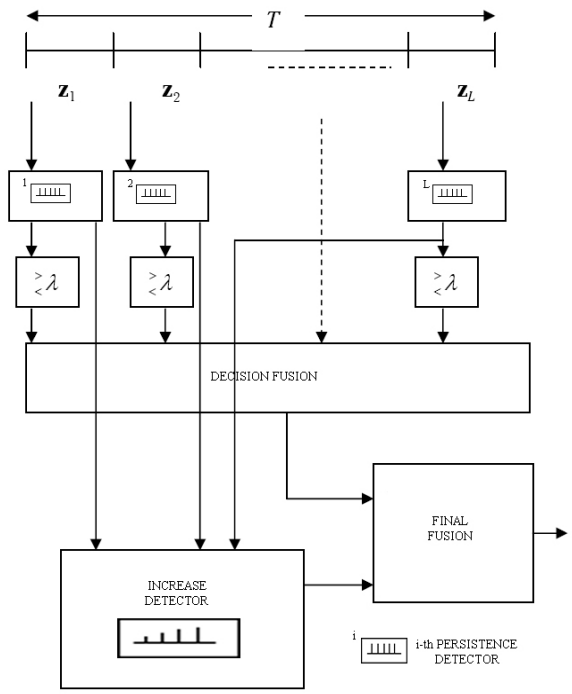

Figure 6. Detector Scheme

Persistence detector allows removing false alarms due to sporadic effects, which behaviour can be assumed to be "high pass". So the persistence detector is implemented by dividing vector **e** into L non-overlapped segments $\mathbf{z_1}$ ... $\mathbf{z_L}$ assuming that the fire signature across each segment is inside a "low pass" subspace with projection matrix **P**. The energy E, inside the subspace **P**, of vector $\mathbf{z_i}$, is compared with a threshold λ that is calculated to meet a desired PFA_0, which is the probability of false alarm for each individual detector (which is equal for all of the chain) in the form of a classic subspace matched filter.

$$E_i = \mathbf{z}_i^T \mathbf{P} \mathbf{z}_i \underset{<}{\overset{>}{\lambda}} \quad (1)$$

To compute the false alarm probability after fusion decision, PFA_p, it is important to define an optimal fusion rule in order to combine the obtained decisions for each of the L segments or detectors of M elements. The optimal decision fusion, as proved in [13], is as follows:

$$R_{opt}(u) = \begin{cases} 1, & \text{, if the number of ones in } \mathbf{u} > nu; \\ 1 \text{ with probability } \gamma, & \text{if the number of ones in } \mathbf{u} = nu; \\ 0, & \text{, if the number of ones in } \mathbf{u} < nu; \end{cases} \quad (2)$$

Where vector $\mathbf{u} = [u_1, \ldots, u_L]^T$ is the vector formed by the individual binary decisions and nu is the number of detectors, from the total number, that we require to meet the persistence criterion.

From this, we get the next expression for PFA_p and PD_p:

$$PFA_p = \sum_{k=nu+1}^{L} \binom{L}{K} PFA_0^k \left(1 - PFA_0\right)^{L-k} + \gamma \binom{L}{nu} PFA_0^k \left(1 - PFA_0\right)^{L-k} \quad (3)$$

$$PD_P = \sum_{k=nu+1}^{L} \binom{L}{k} PD_0^k \left(1 - PD_0\right)^{L-k} + \gamma \binom{L}{nu} PD_0^k \left(1 - PD_0\right)^{L-k} \quad (4)$$

To illustrate the performance of expressions 3 and 4 we have done a simple recreation where we select as input of the persistence detector a continuous level signal under a background noise.

As a result of this simulation we get the ROC curves depicted in Figure 7 and Figure 8.

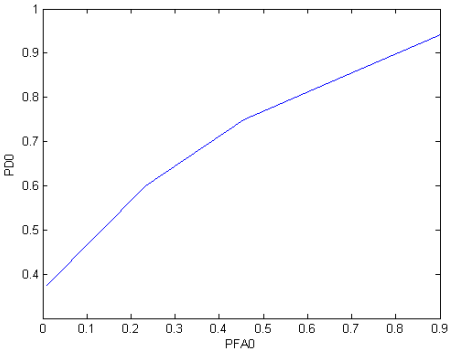

Figure 7. ROC curve PD_o vs PFA_o

The Figure 7 shows the evolution of PD_0 with PFA_0 (note that this curves are for a single detector). The PD_0 has been computed for a range of PFA's between 0.9 and 0.01 with SNR = 1dB and taking for the computation of each PD 1000 Gaussian and correlated vectors of 5 samples size, under a continuous level of signal that depends on the SNR. We can notice, as natural, that if we increase PFA_0 the PD_0 also increase.

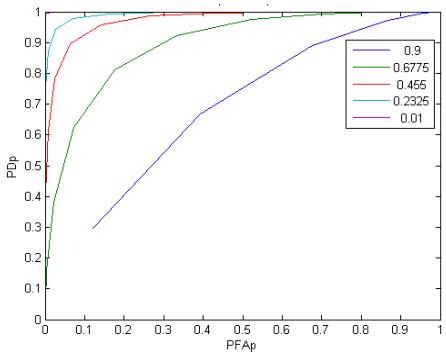

Figure 8. ROC curve: PD_p vs PFA_p with 5 PFA_o's

As regards the ROC curve for the PD_p vs PFA_p (see Figure 8. and comparing it with Figure 7) we can notice that, we get higher values of PD_p for the same PFA_0, and this is due to the fusion decisions.

On the other hand, long time increase detector will enhance the presence of increasing trends. The structure is

based on a filter matched to a continuous component, preceded by a linear transformation $\mathbf{Q}^{(n)}$, which order depends on the speed of fire increasing . It is implemented by looking for increasing trends in the energy vector $\mathbf{z}_E = [E_1...E_L]^T$ where E_i was defined in (1). To this end, the vector $\mathbf{z}_E$ is transformed by a difference matrix of order *n*, $\mathbf{Q}^{(n)}$, and then matched to a continuous component vector of *L-n* elements $\mathbf{s}_n = [1\ldots1\}^T$. The corresponding test is given by [13],

$$\frac{\mathbf{z_E}^T\mathbf{Q}^{(n)T}\left(\mathbf{Q}^{(n)}\mathbf{Q}^{(n)T}\right)^{-1}\mathbf{s_n}}{\sqrt{2p\mathbf{s_n}^T\left(\mathbf{Q}^{(n)}\mathbf{Q}^{(n)T}\right)^{-1}\mathbf{s_n}}} \underset{<}{>} \lambda_0 \tag{5}$$

where the difference matrix is defined by $\mathbf{Q}^{(n)} = \mathbf{Q}_{L-n+1}\cdots\mathbf{Q}_{L-n+1}\cdot\mathbf{Q}_L$ and

$$\mathbf{Q}_L = \begin{pmatrix} -1 & 1 & 0 & \ldots & 0 \\ 0 & -1 & 1 & \ldots & 0 \\ . & . & . & . & . \\ . & . & . & . & . \\ 0 & 0 & \ldots & -1 & 1 \end{pmatrix}_{L,L-1}$$

The threshold λ_0 is calculated to meet a desired *PFA* called PFA_i.

Once described the persistence and increase detectors, we define the final decision rule (final fusion in Figure 6). In a simple way we can formulate the final fusion rule as follows:

$$R(u) = \begin{cases} 1, \text{if } u = [1\ 1] \\ 0, \text{otherwise} \end{cases} \tag{6}$$

Where $\mathbf{u}=[u_p\ u_i]^T$ are the binary random variables that represents the persistence and increase decisions respectively. Although some correlation may exist between both decisions, in a first approximation we can formulate the total PFA and PD as:

$$PFA_t = PFA_p \cdot PFA_i \tag{7}$$

$$PD_t = PD_p \cdot PD_i \tag{8}$$

As presented in next section, some practical simulations have been carried out to corroborate the above equations (3), (4), (7) and (8).

IV. PRACTICAL SIMULATIONS

Settled the theoretical basis and once the design of the system has been considered, some practical simulations are addressed, at this section, to show the correct operation of the proposed system.

Theoretical (continuous line) and experimental curves, obtained by simulation, are superimposed to verify the control on the required *PFA* by fitting parameters *L*, *nu* and PFA_0.

For the experimental curves, we suppose that the input vector is a correlated Gaussian vector of $\mathbf{T} = L \cdot M$ correlated samples taken in *L* segments of size *M* and fixing *M = 6* to simplify.

On the subject of the relation between PFA_p and *nu*, fitting *M*=6, *L*=20, and *nu* varying from 0 to 20 and PFA_0 from 0.5 to 0.01, we have, as expected, that for a fixed PFA_0, when *nu* increases the PFA_p decreases (see Figure 9). Moreover, if the PFA_0 decreases the curves shift to the left, that is, for the same value of *nu* we get a lower PFA_p.

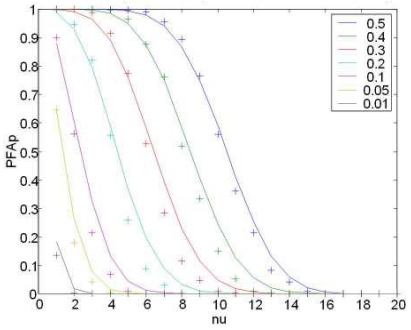

Figure 9. Therotical and practical PFA_p vs *nu* with *L=20* for different PFA_0 values

Regarding the relation between PFA_p and *L* we have fixed a value for *nu=6*, *L* varying from 6 to 20 and PFA_o from 0.5 to 0.01. As depicted in Figure 10. , if we increase the number of segments *L* we have more positive decisions, for a fixed *nu*. For this reason PFA_p increases with *L*.

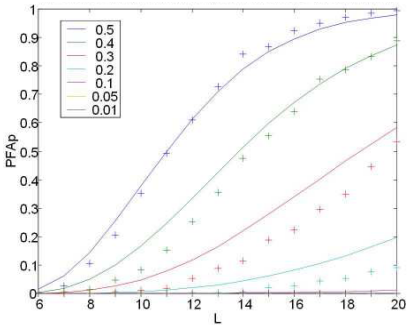

Figure 10. Theoretical and practical PFA_p vs *L* with *nu=6* for diffrerent PFA_0 values

In the case of the relation between PFA_p and PFA_o, we fixed *nu=6*, *L* varying from 6 to 18 and PFA_o from 0.5 to 0.01. Looking at Figure 11. , we can notice that PFA_p

increases with PFA_o. It is a natural result since the probability of false alarm of the fusion follows the same trend that the probability of false alarm of each independent detector.

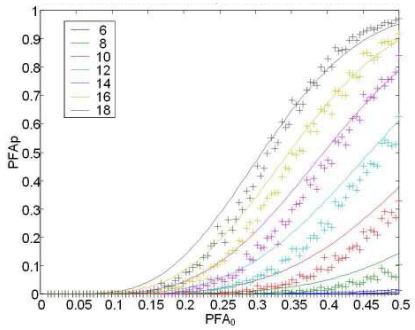

Figure 11. Theoretical and practical PFA_p vs PFA_o with $nu=6$ for different L values

An important conclusion to stress of these simulations is the similar response of theoretical and practical results, thus validating equation (3).

In the case of the dependence of PD_p on the involved parameters by simulation we only depicted practical curves since PD for each detector are known. For these curves we use the same Gaussian vector as input of the scheme, now generating a fire increasing along the T samples. To generate the simulated fire we use a linear model with increase slope, $crec$, the initial value x_{ini} will be recalculated depending on SNR and the noise variance var(x):

$$\mathbf{fire} = x_{ini} + crec \cdot \mathbf{v}' \qquad (9)$$

where $\mathbf{v} = [0, 1, 2, ..., T-1]$, and

$$x_{ini} = \sqrt{10^{\frac{SNR}{10}}} \cdot \mathrm{var}(x) \text{ if } crec > 0 \text{ and } x_{fin} = x_{ini},$$

$$x_{ini} = x_{ini} - crec \cdot (T-1) \text{ if } crec < 0$$

The results were as follows:

Regarding the relation between PD_p and nu as we can see in Figure 12. , fitting L = 10, SNR = 1, and increase slope $crec$ = 0.01, nu varying from 0 to 20 and PFA_0 from 0.5 to 0.01, we have that when nu increases PD_p decreases. That is because when nu increase we have done a more restrictive fusion and we get lower probability of detection.

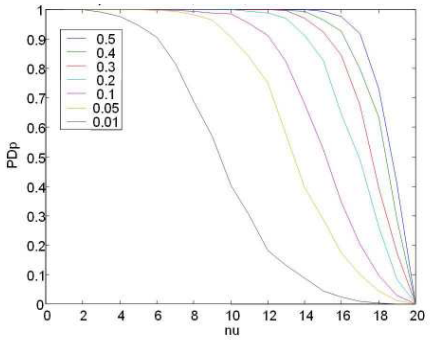

Figure 12. Practical PD_p vs nu with $L=20$, $SNR=1$, $crec=0.01$, for different PFA_0 values

Regarding the relation between PD_p and L (see Figure 13.), fitting nu = 6, SNR=1, and increase slope $crec$ = 0.01, L varying from 6 to 20 and PFA_0 from 0.5 to 0.01, we have that PD_p increases with L, because we have more local decisions to manage in the fusion decision.

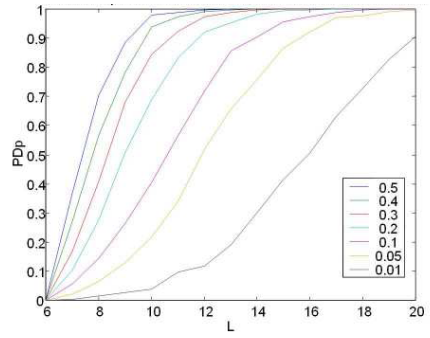

Figure 13. Practical PD_p vs L with $nu=6$, $SNR=1$, $crec=0.01$ for different $PFA0$ values

In the case of the relation between PD_p and PFA_0 we fixed nu = 6, SNR = 1, crec = 0.01, L varying from 6 to 18 and PFA_0 from 0.5 to 0.01. Looking at Figure 14. , we can notice that if PFA_0 increases PD_p also increases, note that PD_p increases quickly in comparison with the curve depicted for one detector (see Figure 7).

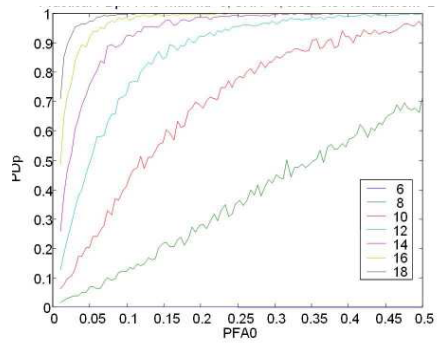

Figure 14. Practical PD_p vs PFA_o with $nu=6$, $SNR=1$, $crec=0.01$ for different L values

Regarding the relation between PD_p and SNR fitting L = 10, nu=6, and increase slope $crec$ = 0.01, SNR varying from 0 to 20 and PFA_0 from 0.5 to 0.01 (see Figure 15.). If the SNR increases the PD increases, this is a natural result, if we increase the signal level we increase the probability of detecting.

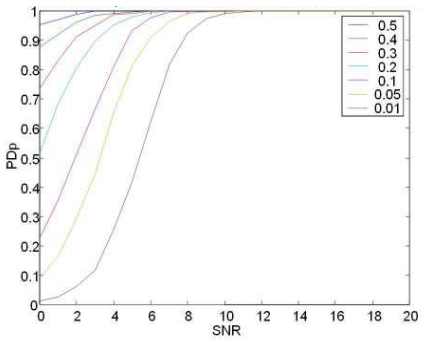

Figure 15. Practical PD_p vs SNR with $L=20$, $SNR=1$, $crec=0.01$, for different PFA_0 values

Another important conclusion to stress from these simulations is the importance of the decision fusion step to improve the PD of only one detector.

In the case of the increase detector, we have no theoretical expressions that connect the PFA_i and PD_i with the model parameters, so we cannot show the curves which compare the theoretical and practical results.

Finally we show the practical and simulated operation of the final decision fusion as a fusion of the persistence detector and the increase detector.

We have also represented the evolution of PFA_t with L in Figure 16. and with PFA_0 in the Figure 17. for a fixed value of nu.

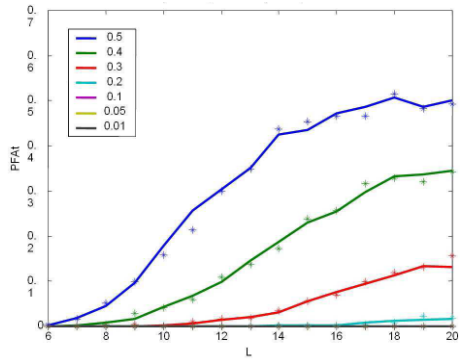

Figure 16. Theoretical and practical PFA_t vs L with different PFA_0 values

As expected, we can see in Figure 16. , as if we increase the value of segments L we have more positive decisions, for a fixed nu, and this increases the PFA_t.

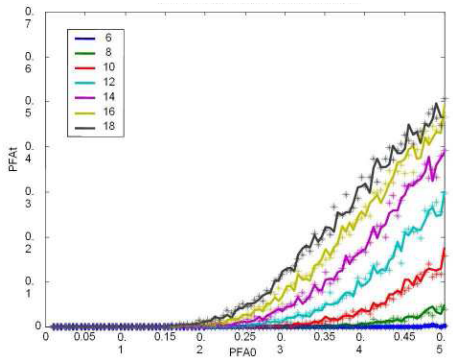

Figure 17. Theoretical and practical PFA_t vs PFA_0 for different L values

In the case of Figure 17. occurs something very similar, increasing the probability of false alarm of each independent detector PFA_0 increases the probability of false alarm of the fusion PFA_t and more significantly by increasing L.

In the same way, in Figures 18, 19 and 20 we have represented the evolution of PD_t with L, PFA_0, and SNR thus corroborating the concordance between the practical and theoretical results.

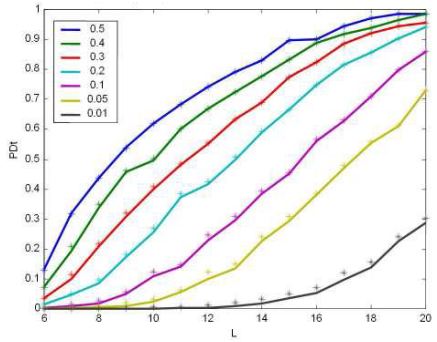

Figure 18. Theoretical and practical PD_t vs L with $SNR=1$, $crec=0.01$ for different PFA_0 values

In Figure 18, if we increase the number of segments L we have more local decisions and this increases the PD_t .

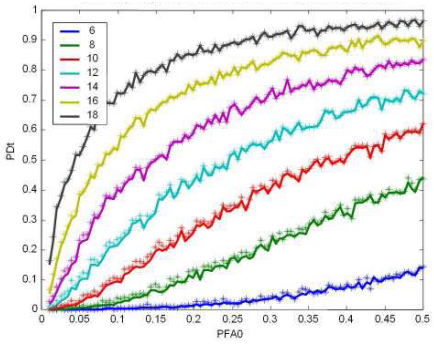

Figure 19. Theoretical and practical PD_t vs PFA_o with nu=6, $SNR=1$, $crec=0.01$ for different L values

In Figure 19, if we increase the probability of false alarm of each independent detector PFA_0 the PD_t increases.

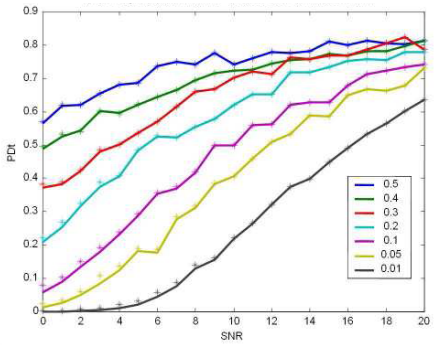

Figure 20. Theoretical and practical PD_t vs *SNR* with $L=10$, $crec=0.01$ for different PFA_0 values

In Figure 20, if we increase the signal to noise ratio *SNR* the PD_t increases because we increase the probability of detecting.

Moreover, if we compare the continuous and dotted lines we can notice that the practical results are perfectly fitted to the theoretical ones.

Equations (7) and (8) also verify thus, indicating that the assumed uncorrelation between the increase and persistence detector is an appropriate hypothesis.

Another important issue to take into account is the capability of the system to make an early detection of fire. The curve depicted in Figure 21 have been computed for a fixed L=10, and PFA_0, PFA_i varying from 10^{-3} to 10^{-6} and show the delay that the system requires to generate the first fire alarms from the beginning of the fire.

We can conclude that for a fixed value of L, if *nu* is decreased L-nu increases and the persistence decision fusion is less restrictive and the fire can be detected earlier. For a fixed value of *L-nu*, if the PFA_0 is increased, the system response speed increases.

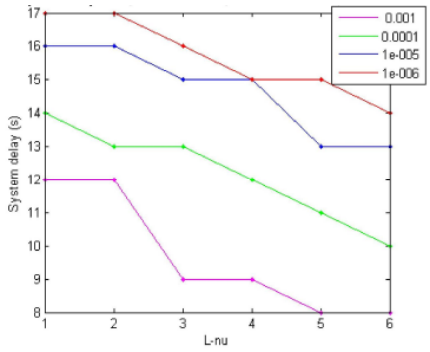

Figure 21. System delay vs L-nu, for fire detection with diferent PFA_0

We can conclude that the system performs an earlier detection like tens of seconds, if we compare the system response with that of the average watchman.

V. RESULTS IN A REAL ENVIRONMENT

Some results in a real environment were shown to demonstrate the correct operation of the proposed system.

First, the system was tested under various real scenarios by performing the capture of infrared images from real area-controlled forest fires under the supervision of several firemen. Specifically in two tests with controlled fires made in Ayora and Alcoy parks.

The signal processing parameters were: L=10, *nu*=2, $PFA_0 = PFA_i = 10^{-3}$. One of the processing testing resut was shown in Figure 22. In this test we can see how the processing system is capable of discerning possible unwanted effects due to other hot zones detected by the thermal camera. In this example, the fire was detected at 1500 m of direct vision.

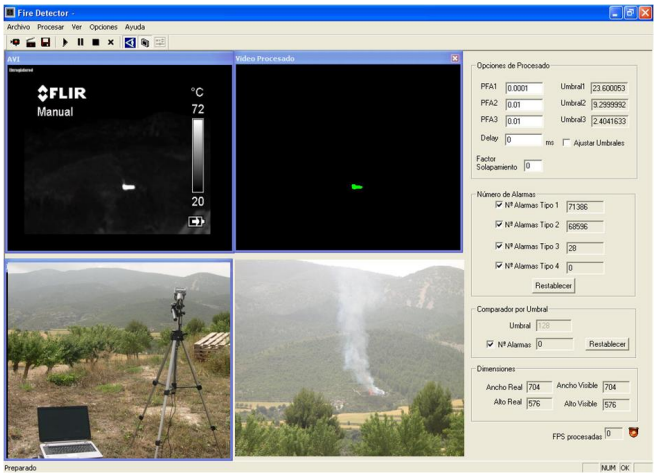

Figure 22. *System tested in a real scenario*

Finally the system was installed in the natural park named "El Carrascal de la Font Roja" in the Spanish city of Alcoy. The Font Roja natural park area is about 2500 hectares, and its maximum altitude is 1352 m.

Specifically it was installed in the tower of the "Sanctuary of the Red Font" building, see Figure 23.

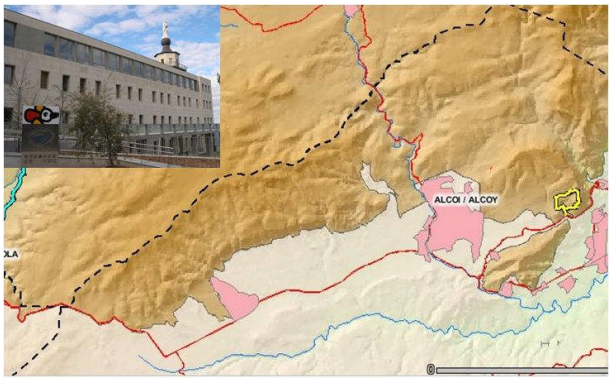

Figure 23. Natural park named "El Carrascal de la Font Roja"

During its normal operation, the system has generated true detections (see Figure 24.) and false alarms (see Figure 25.).

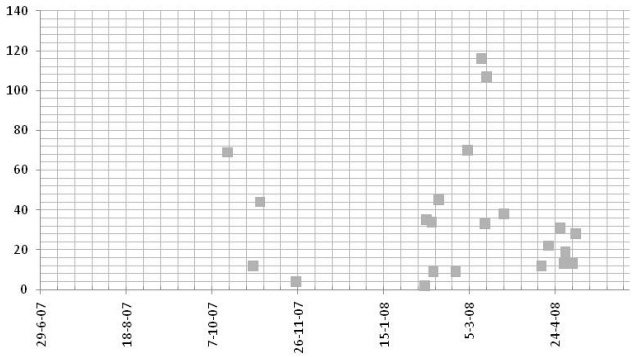

Figure 24. True alarms/day

A true detection is defined as an alarm that can be associated a posteriori to a true fire (whether or not the areas is under human control). On the other hand, a false alarm is one that cannot be associated to a real fire. And it is therefore a system error.

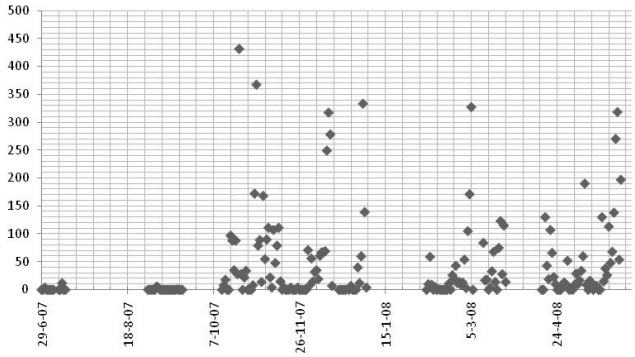

Figure 25. False alarms/day

A small average number of 40 false alarms per day were produced, which is in concordance with the configured value of PFA_t of approximately 8E-9.

Some possible explanations can be found for the false alarms. Many of them were produced during the night or in especially cool weather conditions in the presence of fog. Other false alarms were produced during the night by the lights of the city of Alcoy (part of the scanning angle included this city). Finally, some false alarms were observed on sunny days that had alternate periods of clouds.

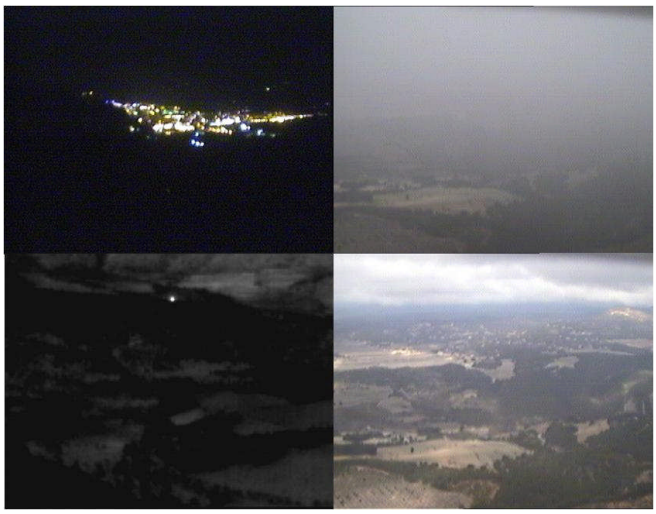

Figure 26. Thermal and visible images of false alarms examples

These results are due to the automatic calibration of the infrared camera. When the average infrared energy level is very low, the camera increases the sensitivity, so more false alarms are to be expected.

Appropriate control of the automatic calibration of the camera by means of a temperature sensor could avoid most of these false alarms. Then, if these problems are resolved, this amount of false alarms will be reduced drastically, theoretically getting average values of 14 false alarms per day or a PFA_t of 3E-9.

On the other hand the system has generated many true fire alarms (see examples in Figure 27.).

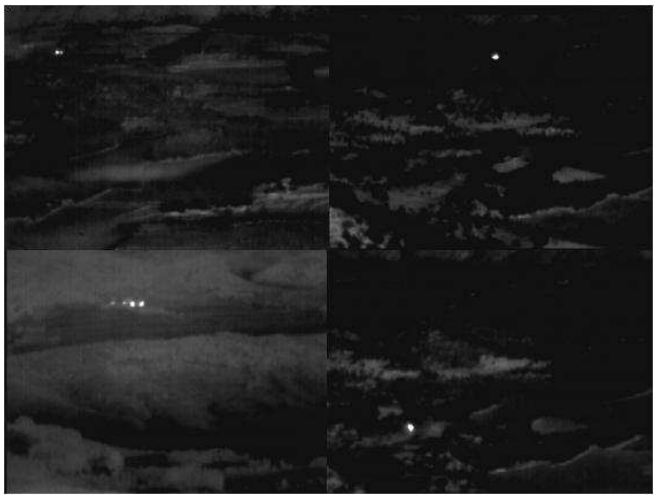

Figure 27. Thermal images of detection examples

Most of the true fires were detected from a significant distance approximately 1 to 10 km. To our knowledge, no fires went undetected during this period.

VI. CONCLUSIONS

A system for early forest fire detection based on images obtained from an infrared sensor network, has been presented. The system is based on the use of several sensors strategically located to render a required coverage.

We have focus on processing the images captured from the infrared sensors. Particularly interesting is the fusion of two decisions respectively corresponding to persistence and an increase detector. In essence both detectors try to reproduce the behavior of a human watchman: an uncontrolled fire must persist at short-term, and must increase at long-term.

The correct operation of the system has been justified verifying that the final *PFA* may be controlled by appropriate selection of the detector parameters. We have also evaluated that the theoretical *PD* for the total fusion decisions is consistent with practical simulations, and we can stress from here the advantage of decision fusion.

The functionality of the system has been verified in diverse controlled real tests and in normal operation in order to authenticate the accuracy of the proposed system. We have shown the temporary evolution of false alarms and true detections to evaluate the performance of the system in the real environment. We have also evaluated the delay of the system in order to generate an alarm corresponding to a real fire.

The obtained results show large potential interest for this system to replace human surveillance. Furthermore, and once it has been justified the correct operation of each single sensor, it is important to emphasize the importance of a network sensor in order to increase the coverage area of the system. [14]

ACKNOWLEDGMENT

This work has been supported by Generalitat Valenciana, under grant GVEMP06/001.

REFERENCES

[1] I. Bosch, S. Gómez, and L. Vergara, “Automatic forest surveillance based on infrared sensors”, Proc. 2007 International Conference on Sensor Technologies and Applications, (SENSORCOMM 2007), pp 572-577. 0-7695-2988-7/07

[2] E. Pastor, L. Zárate, E. Planas, and J. Arnaldos, “Mathemaical models and calculation systems for the study of wildland fire behaviour”. Prog Energy Combust Sci, 29, pp 139 – 152. 2003.

[3] Y. Rauste, E. Herland, H. Frelander, K. Soini, T. Kuoremaki, and A. Ruokari “Satellite-based forest fire detection for fire control in boreal forests”. International Journal of Remote Sensing, Vol. 18, no. 12, pp. 2641 - 2656, 1997.

[4] M.J. Carlotto, “Detection and analysis of change in remotely sensed imagery with applications to wide area surveillance”, IEEE Trans. Image Procees. Volume 6, no 1, pp. 189-202, 1997.

[5] Jin Li, Qingwen Qi, Xiuping Zou, Hu Peng, Lili Jiang, and Yajuan Liang, “Technique for automatic forest fire surveillance using visible ligth image”. Proc. on the IGARSS ´05. Volume 5, pp. 3135 - 3138, July 2005

[6] Y. Dedeoglu, B. Toreyin, U. Güdkübay, A. Enis, and C. Etin, “Real-time fire and flame detection in video”. IEEE 30th International Conference on Acustics, Speech and Signal Processing (ICASSP), pp: 669-672. 2005

[7] B.C. Arrue, A. Ollero, and J.R. Matinez de Dios, “An intelligent system for false alarm reduction in infrared forestfire detection”. IEEE Intelligent Systems. Volume: 15, no 3, pp. 64-73, 2000.

[8] J. Vicente and P. Guillemant, “An image processing technique for automatically detecting forest fire”, Int J. Therm. Sci, 41, pp: 1113-1120, 2002.

[9] S. Briz, J.A. De Castro, J.M. Aranda, J. Meléndez, and F. López, “Reduction of false alarm rate in automatic forest fire infrared surveillance systems”, Remote sensing of Envionment, 86, pp: 19-29. 2003

[10] L.Vergara and P.Bernabeu, “Automatic Signal Detection applied to fire control by infrared digital signal processing”. Signal Processing. Volume 80, pp. 659-669, 2000.

[11] L.Vergara and P.Bernabeu, “Simple approach to nonlinear prediction” Electronic Letters. Volume 37, no 14, pp. 926-928. July 2001.

[12] P.Bernabeu, L.Vergara, I.Bosch, and J.Igual, “A prediction/detection scheme for automatic forest fire surveillance”. Digital Signald Processing. Volume 14, pp. 481-507, 2004.

[13] I. Bosch and L. Vergara, “Forest Fire Detection by Infrared Data Processing”. Data Fusion for Situation Monitoring, Incident Detection and Response Management, 198 NATO Science Series: Computer & Systems Sciences. Editor E. Shahbazian, G. Rovina, P. Valin, IOS Press, Volume 6, pp. 931-944, 2006.

[14] J. Lloret, M. Garcia, D. Bri, and S. Sendra, “A Wireless Sensor Network Deployment for Rural and Forest Fire Detection and Verification”, Sensors, Vol. 9, Issue 11, Pp. 8722-8747. October 2009.